Journal of Materials Chemistry C

Naphthalene Core-Based Noncovalently Fused-ring Electron Acceptors: Effect of Linkage Positions on Photovoltaic Performances

Journal:	*Journal of Materials Chemistry C*
Manuscript ID	TC-COM-09-2019-005013.R2
Article Type:	Communication
Date Submitted by the Author:	15-Nov-2019
Complete List of Authors:	Zheng, Rui; Beijing Normal University Guo, Qingxin; Beijing Normal University Hao, Dan; Beijing Normal University Zhang, Cai'e; Beijing Normal University, Xue, Wenyue; Xi'an Jiaotong University, State Key Laboratory for Mechanical Behavior of Materials Huang, Hao; Beijing Normal University Li, Cuihong; Beijing Normal University, Institute of Polymer Chemistry & Physics, College of Chemistry; Ma, Wei; Xi'an Jiaotong University, State Key Laboratory for Mechanical Behavior of Materials Bo, Zhishan; Institute of Polymer Chemistry & Physics, College of Chemistry

Journal Name

COMMUNICATION

Naphthalene Core-Based Noncovalently Fused-ring Electron Acceptors: Effect of Linkage Positions on Photovoltaic Performances

Received 00th January 20xx,
Accepted 00th January 20xx

DOI: 10.1039/x0xx00000x

www.rsc.org/

Rui Zheng,‡[a] Qingxin Guo,‡[a] Dan Hao,[a] Cai'e Zhang,[a] Wenyue Xue,[b] Hao Huang,[a] Cuihong Li,*[a] Wei Ma,*[b] Zhishan Bo*[a]

Two mutually isomeric noncovalently fused-ring electron acceptors (NC-FREAs) NOC6F-1 and NOC6F-2 containing two cyclopentadithiophene (CPDT) moieties linked at the 2,6 or 1,5 positions of naphthalene ring were designed and synthesized for organic solar cells (OSCs). Intramolecular noncovalent S···O interactions were introduced to NOC6F-1 and NOC6F-2. The tiny structural variation for NOC6F-1 and NOC6F-2 by just changing the linkage positions affects largely the molecular configuration, absorption, molecular packing, charge transport and photovoltaic performance. Compared to NOC6F-2, NOC6F-1 exhibits smaller distortions between cyclopentadithiophene and the naphthalene unit, leading to an extended conjugation and enhanced π-π stacking. NOC6F-2 exhibits a poor planarity, which restricts the electron delocalization as well as densely π-π stacking in film. When blended with PBDB-T, NOC6F-1 exhibits more orderly stacking both along the out-of-plane and in-plane direction than NOC6F-2. OSCs based on PBDB-T:NOC6F-2 merely showed a power conversion efficiency (PCE) of 6.74% with lower J_{sc} and FF. OSCs based on NOC6F-1 achieved a higher J_{sc} of 17.08 mA cm^{-2} and an FF of 65.79%, thus leading to a significantly enhanced PCE of 10.62%. These results indicate that the acceptor molecules with a planar molecular backbone is an important design strategy for NC-FREAs.

Introduction

Non-fullerene acceptors (NFAs) have drawn significant attention for application in organic solar cells (OSCs) due to their distinct advantages such as broad and strong absorption[1-4] and tunability of energy levels.[5-8] Hitherto, power conversion efficiencies (PCEs) of NFAs based OSCs have reached over 16% for single junction[9-11] and 17% for tandem devices.[12] NFAs with acceptor-donor-acceptor (A-D-A) molecular architecture are in particular interesting because of their stronger light-harvesting capability in the visible to near-infrared region.[13-15] Most OSCs with PCE exceeding 11% employ A-D-A type small molecular acceptor.[16-20] The central D units are usually fused-ring structures such as indacenodithiophene (IDT), indacenodithieno[3,2-b]thiophene (IDTT) and so on. Such fused-ring electron acceptors (FREAs) usually possess a planar molecular structure, which is beneficial for efficient electron delocalization, face-on molecular arrangement, and charge transport in OSCs.[21-25] However, the syntheses of such FREAs are challenging, often encounter complicated synthesis, low yields and multi-step purification.[26, 27]

The noncovalently interactions, such as O···S, O···H, H···F, S···S, S···F and so on, have been used in developing high-performance organic semiconductors.[28, 29] Recently, a series of A-D-A type NFAs incorporating noncovalently interactions have been synthesized and applied in OSCs. Similar to covalently fused-ring acceptors, noncovalently fused-ring electron acceptors (NC-FREAs) can also possess a planar ladder-like structure and good solubility.[30] Broad absorption, efficient charge transport, exciton separation and PCEs comparable to FREAs can also be achieved for NC-FREAs.[31-34] So far, the optimized OSCs based on NC-FREAs have displayed an outstanding PCE of above 13% for single junction devices.[35] More importantly, complicated synthesis and low yield can be skillfully avoided. These results reveal that the strategy of incorporating noncovalently interactions into non-fullerene molecular acceptors has huge potential for low-cost high-performance OSCs.

To further enhance the photovoltaic performance of NC-FREAs based OSCs, it is still meaningful to explore the effect of molecular backbone, end-groups and side chains on the absorption, energy level, charge mobility and morphology. In addition, "isomeric effect", which has been widely explored in organic field-effect transistors and FREAs,[19, 36-39] is also valuable for being explored for NC-FREAs. On the basis of these considerations, herein, by virtue of noncovalent S···O interactions we designed and synthesized two mutually

[a] Key Laboratory of Energy Conversion and Storage Materials, College of Chemistry, Beijing Normal University, Beijing 100875, China. E-mail: licuihong@bnu.edu.cn; zsbo@bnu.edu.cn
[b] State Key Laboratory for Mechanical Behavior of Materials, Xi'an Jiaotong University, Xi'an 710049, China. E-mail: msewma@mail.xjtu.edu.cn
†Electronic Supplementary Information (ESI) available. See DOI: 10.1039/x0xx00000x
‡ These authors contributes equally to this work.

isomeric NC-FREAs **NOC6F-1** and **NOC6F-2**, which are composed of two cyclopentadithiophene (CPDT) moieties linked at 2,6 or 1,5 positions of naphthalene ring and two monofluorinated 1,1-dicyanomethylene-3-indanone electron-withdrawing end groups. Their absorption property, molecular packing and charge transport behavior were extensively investigated. Compared with **NOC6F-2**, **NOC6F-1** exhibited an enhanced planarity, closer π-π stacking distance and extended absorption. The as-cast devices based on PBDB-T:**NOC6F-1** exhibited a superior PCE of 10.62% with a higher J_{sc} of 17.08 mA cm^{-2} and an FF of 65.79%. For the OSCs based on PBDB-T:**NOC6F-2**, the PCE can only reach 6.74% due to the lower J_{sc} of 13.21 mA cm^{-2} and FF of 53.26%. Our studies have demonstrated that NC-FREAs are promising for achieving high performance organic solar cells.

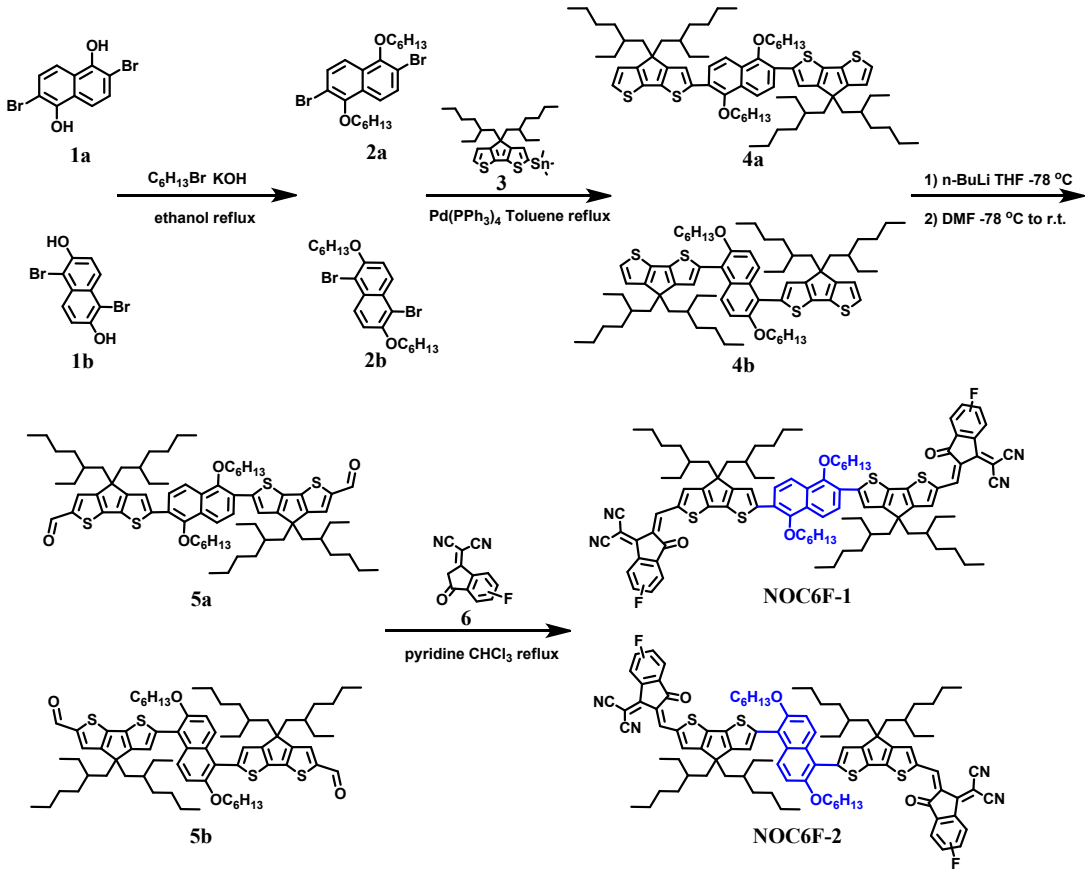

Scheme 1 Synthetic routes to **NOC6F-1** and **NOC6F-2**.

Results and discussion

Material synthesis and characterization

The synthetic routes of **NOC6F-1** and **NOC6F-2** are displayed in Scheme 1 and the detailed information are provided in the supplementary information (SI). Taking 2,6-dibromo-naphthalene-1,5-diol (**1a**) and 1,5-dibromonaphthalene-2,6-diol (**1b**) as starting materials, compound **2a** and **2b** were obtained by alkylation of **1a** and **1b** with 1-bromohexane in yields of 73% and 77%, respectively. Stille coupling of compound **3** with **2a** and **2b** afforded compounds **4a** and **4b**, respectively, in yields of approximately 95% using $Pd(PPh_3)_4$ as the catalyst precursor. Compounds **4a** and **4b** were subjected to lithiation with *n*-BuLi in anhydrous tetrahydrofuran under the condition of -78 °C, and the formed dianions were subsequently quenched by anhydrous *N,N*-dimethylformamide (DMF) to afford compounds **5a** and **5b** in yields of 90% and 86%, respectively. **NOC6F-1** and **NOC6F-2** were prepared in yields of 59% and 55%, respectively, by Knoevenagel condensation of **5a** and **5b** with compound **6**. **NOC6F-1** and **NOC6F-2** exhibited excellent solubilities in common organic solvents such as chloroform (CF), chlorobenzene (CB) and *o*-dichlorobenzene (DCB). Differential Scanning Calorimeter (DSC) was measured at a heating or cooling rate of 10 °C min^{-1} and the curves showed no obvious crystallization or melting peak in the range of 80 to 300 °C (Fig. S1). Besides, it is observed from thermogravimetric curves (Fig. S2) that the decomposition temperatures (5% weight loss) of **NOC6F-1** and **NOC6F-2** are 329 and 348 °C respectively, indicating that **NOC6F-1** and **NOC6F-2** are of good thermal stabilities.

DFT calculations

The molecular geometry conformation of **NOC6F-1** and **NOC6F-2** were simulated using density functional theory (DFT) at B3LYP/6-31G(d) level. The long alkyl chains were replaced with

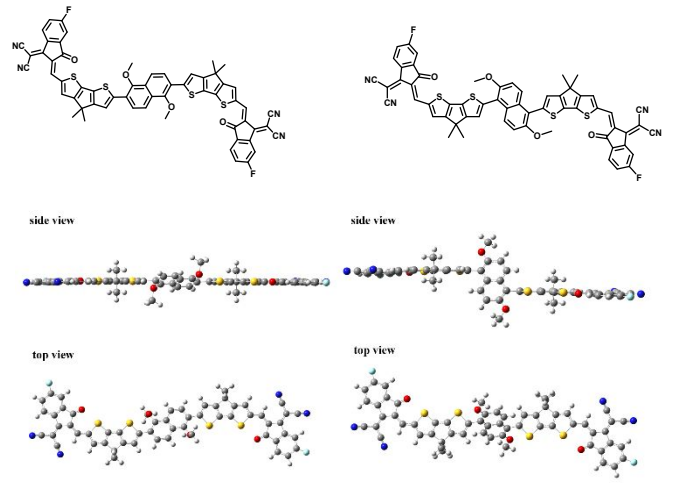

Fig. 1 Simulated molecular geometries obtained by DFT calculations for **NOC6F-1** and **NOC6F-2** in simplified mode.

methyl groups to simplify the simulation procedure. As shown in Fig. 1, **NOC6F-1** and **NOC6F-2** exhibited torsion structures with the dihedral angles between the central naphthalene core and the cyclopentadithiophene (CPDT) unit of 20° and 58°, respectively. The dihedral angles originate from the steric hindrance of hydrogen atoms on the naphthalene core and adjacent thiophene ring. **NOC6F-1** exhibited a smaller torsion angle than **NOC6F-2**, the reason is that the steric hindrance of the β position is weaker than the α position due to the para-H (α-H) of naphthalene unit pointing directly towards CPDT unit in **NOC6F-2**. **NOC6F-1** is almost of planar conformation because of the intramolecular noncovalent S···O interactions. Enhanced planarity is conducive to good conjugation and intermolecular π-π interactions.[30] Besides, the highest occupied molecular orbital (HOMO) and the lowest unoccupied molecular orbital (LUMO) levels of **NOC6F-1** and **NOC6F-2** were also calculated and the results are shown in Fig. S3. The LUMO of **NOC6F-1** has an electron density spreading across the entire molecule, while the electron density of the LUMO in **NOC6F-2** is localized near the ending group due to the decrease in effective conjugation.

Optical properties

The UV-vis absorption properties of the two acceptor molecules are presented in Fig. 2 and Table 1. In the CF solutions, these two acceptors exhibit featureless absorption band in the range of 500 to 750 nm with a peak at 690 nm for **NOC6F-1** and 632 nm for **NOC6F-2**, which may be attributed to their flexible and rotational conformation in solutions. The maximum molar extinction coefficients were determined to be 2.24×10^5 and 1.95×10^5 M^{-1} cm^{-1} for **NOC6F-1** and **NOC6F-2**, respectively. Ingoing from solution to film, **NOC6F-1** showed a broader and structured absorption with two peaks at 665 and 717 nm, suggesting its aggregation in film. However, as for **NOC6F-2**, it only exhibited a slightly broader absorption with the absorption peak slightly blue-shifted to 627 nm, indicating it form amorphous structure in film. These results indicate the tiny structural variation by just changing the linkage positions affects largely the molecule absorption and aggregation behaviors in film. According to the formula $E_{g,opt} = 1240/\lambda_{onset}$, the optical bandgaps ($E_{g,opt}$) deduced from the absorption edges (λ_{edge}) are 1.58 and 1.68 eV for **NOC6F-1** and **NOC6F-2**, respectively. In addition, the broad absorption of **NOC6F-1** is complementary to that of PBDB-T, indicating the blend of PBDB-T:**NOC6F-1** can capture a wider range of light.

Electrochemical properties

Cyclic voltammetry (CV) was carried out to explore the electrochemical properties of **NOC6F-1** and **NOC6F-2**. Ferrocene was chosen as an internal reference. The onset oxidation ($E_{onset,\ ox}$) and reduction potentials ($E_{onset,\ red}$) can be measured from the cyclic voltammograms as shown in Fig. 2c. By using the equation of $E_{HOMO/LUMO} = -e(E_{onset,ox/red} - E_{Fc/Fc+} + 4.80)$ eV, the HOMO energy levels were calculated to be -5.55 and -5.50 eV for **NOC6F-1** and **NOC6F-2**, respectively. The LUMO energy levels were determined to be -3.77 and -3.72 eV for **NOC6F-1** and **NOC6F-2**, respectively. The higher LUMO energy level of **NOC6F-1** and **NOC6F-2** will be beneficial for high V_{oc} in OSCs. The electrochemical data of the two NC-FREAs are summarized in Table 1, and the energy level diagram is shown in Fig. 2d.

Photovoltaic properties

The photovoltaic performances of these two target acceptors were evaluated with an inverted solar cell structure of ITO/ZnO/donor:acceptor/MoO_3/Ag. PBDB-T was chosen as the donor due to the favorable absorption complementary to **NOC6F-1**. Various conditions were carefully explored such as D/A ratio, film thickness, additive and annealing temperature. The optimized device parameters are summarized in Table 2 and the corresponding current density-voltage (*J-V*) curves are displayed in Fig. 3a. **NOC6F-1** and **NOC6F-2** displayed quite different photovoltaic performance. The OSCs based on PBDB-T:**NOC6F-1** exhibited the highest PCE of 10.62% with a V_{oc} of 0.95 V, J_{sc} of 17.08 mA cm^{-2} and an FF of 65.79% without any additive or post-treatment. However, the optimized OSCs based on **NOC6F-2** afforded only a low PCE of 6.74% with a V_{oc} of 0.96 V, J_{sc} of 13.21 mA cm^{-2} and an FF of 53.26%. In addition, the high V_{oc} for **NOC6F-1** and **NOC6F-2** based devices is related to their high LUMO levels. For PBDB-T:**NOC6F-1** based device, the high J_{sc} benefits from its broader absorption and the high FF value is due to its favorable carrier transport property (vide infra).

External quantum efficiency (EQE) curves of PBDB-T:**NOC6F-1** and PBDB-T:**NOC6F-2** based devices were measured under monochromatic light and the curves are shown in Fig. 3b. The PBDB-T:**NOC6F-1** based devices showed a photocurrent response in the range of 300 to 800 nm, which is stronger and broader than that of PBDB-T:**NOC6F-2** based ones, agreeing well with their film absorption spectra. The calculated J_{sc} values from the integration of EQE curves are consistent with those from *J-V* measurements.

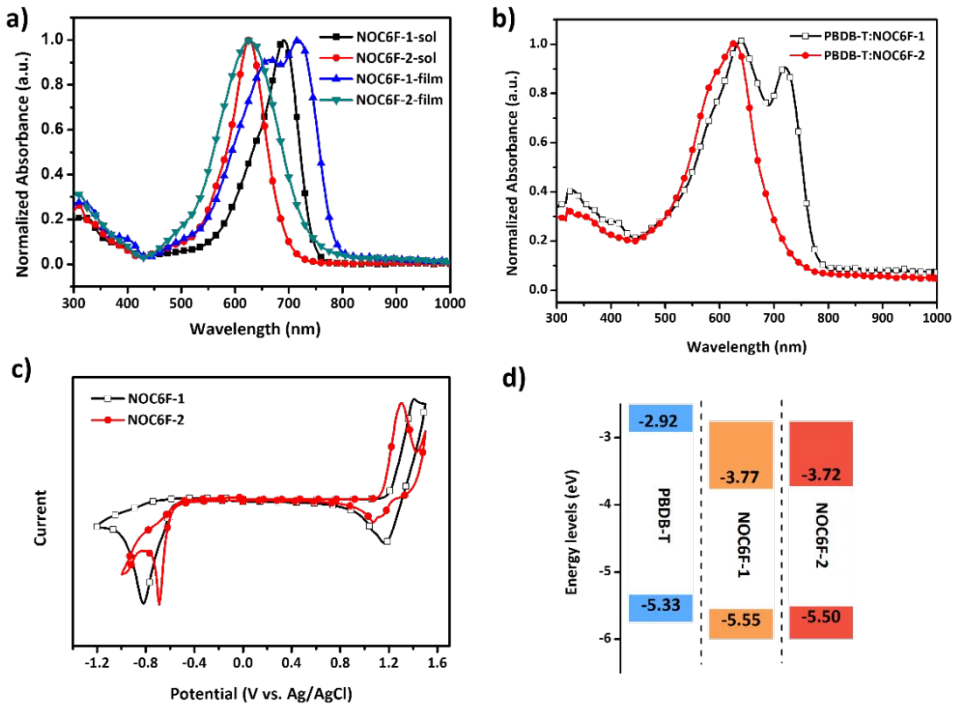

Fig. 2 a) Normalized UV–vis spectra of **NOC6F-1** and **NOC6F-2** in CF solutions and in films; b) Normalized UV–vis spectra of PBDB-T:**NOC6F-1** and PBDB-T:**NOC6F-2** blend films; c) Cyclic voltammograms of **NOC6F-1** and **NOC6F-2** and d) Energy levels of **NOC6F-1**, **NOC6F-2** and PBDB-T.

Table 1 Absorption and energy levels of **NOC6F-1** and **NOC6F-2**.

Acceptor	Solution ($CHCl_3$)			Film		E_g^{opt} [eV]	HOMO [eV]	LUMO [eV]	E_g^{cv} [eV]
	λ_{peak} [nm]	λ_{edge} [nm]	ε [M^{-1} cm^{-1}]	λ_{peak} [nm]	λ_{edge} [nm]				
NOC6F-1	690	745	2.24×10^5	665 717	784	1.58	-5.55	-3.77	1.78
NOC6F-2	632	698	1.95×10^5	627	736	1.68	-5.50	-3.72	1.78

Charge mobilities

The hole mobility and the electron mobility of the blend films were determined by SCLC method (shown in Fig. S5) and the results are summarized in Table S4. For the PBDB-T:**NOC6F-1** film, the hole and electron mobilities are 2.56×10^{-3} and 2.07×10^{-3} cm^2 V^{-1} s^{-1}, respectively, with the μ_e/μ_h value of 0.81. The PBDB-T:**NOC6F-2** film exhibits hole and electron mobilities up to 8.39×10^{-4} and 6.02×10^{-4} cm^2 V^{-1} s^{-1}, respectively, with the μ_e/μ_h value of 0.72. The results indicate that PBDB-T:**NOC6F-1** blend film has higher and more balanced charge transport capability, which is consistent with the J_{sc} and the FF of their devices.

Recombination Dynamics

The exciton dissociation probability in the OSCs devices was investigated by measuring photocurrent density (J_{ph}) versus the effective voltage (V_{eff}) and the curves are shown in Fig. 3c. J_{ph} is defined as photocurrent density difference between illuminated (J_L) and dark (J_D) situations. V_{eff} equals V_0 - V, where V_0 is the voltage at which photocurrent reaches zero and V is the applied voltage. When J_{ph} reaches saturation (J_{sat}), it suggests that the exciton dissociation reaches the maximum level, and the charges almost collected by the electrodes.[40] The charge dissociation probabilities (P(E, T)), calculated from J_{ph}/J_{sat}, of **NOC6F-1** and **NOC6F-2** based OSCs, are 0.95 and 0.88, respectively, indicating more efficient exciton dissociation and charge collection efficiencies occurred in **NOC6F-1** based OSCs than **NOC6F-2** based ones. To further understand the charge recombination behaviors of **NOC6F-1** and **NOC6F-2** based solar cells, J_{sc} under different light intensity (P) (Fig. 3d) are measured. The correlation between J_{sc} and P_{light} can be described by the equation $J_{sc} \propto P^{\alpha}$. When $\alpha = 1$, it implies that no bimolecular recombination occurs. If $\alpha < 1$, it indicates the existence of bimolecular recombination.[5] The α values of PBDB-T:**NOC6F-1** and PBDB-T:**NOC6F-2** blend films are 0.92 and 0.87, respectively, demonstrating that **NOC6F-1** based OSCs can better impede the bimolecular recombination than **NOC6F-2** based ones, in accordance with the improved FF of PBDB-

T:**NOC6F-1** based devices compared with PBDB-T:**NOC6F-2** based ones.

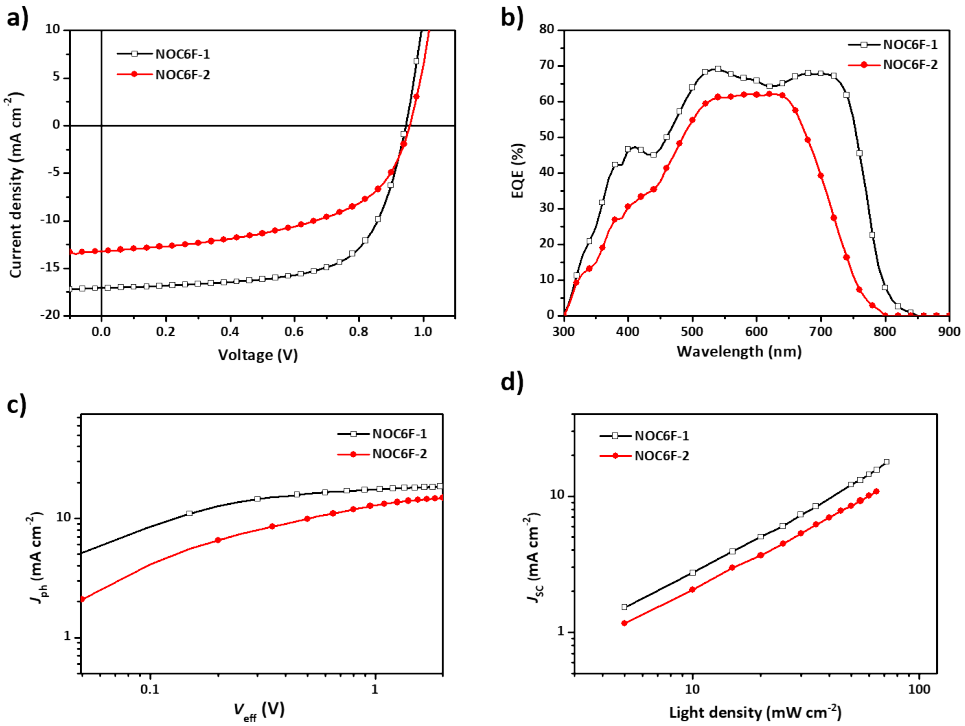

Fig. 3 a) *J-V* and b) EQE c) J_{ph} versus V_{eff} and d) J_{sc} versus light density curves for **NOC6F-1** and **NOC6F-2** based OSCs.

Table 2 The optimal photovoltaic parameters of PBDB-T:**NOC6F-1**/**NOC6F-2** based devices.

Active layer [a]	V_{oc} [V]	J_{sc} [mA cm^{-2}]	calculated J_{sc} [mA cm^{-2}]	FF [%]	PCE [%]
PBDB-T:**NOC6F-1**	0.95	17.08	15.74	65.79	10.62 (10.29 ± 0.33) [b]
PBDB-T:**NOC6F-2**	0.96	13.21	11.58	53.26	6.74 (6.58 ± 0.16) [b]

[a] PBDB-T:acceptor = 1:1.2 (w/w); [b] Average PCEs are obtained from 10 devices.

Non-radiative recombination losses

The non-radiative recombination losses in OSCs often constitute a significant part of the total energy losses, which are usually higher than that in inorganic or perovskite solar cells.[41-43] The non-radiative energy losses are related to the external quantum efficiency of electroluminescence (EQE_{EL}) via the equation $q\Delta V_{non-rad} = -kT\ln(EQE_{EL})$, where q is the elementary charge, k is the Boltzmann constant and T is temperature.[44] To further study the non-radiative recombination losses for **NOC6F-1** or **NOC6F-2** based OSCs, EQE_{EL} are measured and the non-radiative recombination losses are 0.275 eV for **NOC6F-1** and 0.286 eV for **NOC6F-2** (Fig. S7), indicating similar and low non-radiative recombination losses for both OSCs, which are comparable with amorphous Si or perovskite solar cells.[41, 42, 45]

Morphology characterization

Atomic force microscope (AFM) and transmission electron microscope (TEM) experiments were performed to explore the morphological characteristics of the active layers. The AFM images (Fig. S8a and S8b) indicates that PBDB-T and these two acceptors have a good miscibility in the blend films, and the active layers are smooth with relatively low root-mean-square (RMS) roughness values of 1.56 nm for PBDB-T:**NOC6F-1** and 1.33 nm for PBDB-T:**NOC6F-2**, respectively. In the TEM images as shown in Fig. S8c and S8d, fibril structures, which are beneficial to charge carrier generation and transportation,[46-48] can be observed for both blend films. Besides, to investigate the molecular orientation and stacking behavior in the blend film, grazing-incidence wide-angle X-ray scattering (GIWAXS) was measured and the results are shown in Fig. 4. In the out-of-plane direction, the pristine PBDB-T presents a π-π stacking (010) peak at q_z = 1.67 Å^{-1}, corresponding to a *d* of 3.76 Å. For the PBDB-T:**NOC6F-1** blend film, an enhanced π-π stacking (010) peak at q_z = 1.65 Å^{-1} (*d* = 3.80 Å) emerged, suggesting that **NOC6F-1** exhibits a closely ordered face-on packing. On the contrary, for the PBDB-T:**NOC6F-2** blend film, the (010) peak (q_z = 1.64 Å^{-1}, *d* = 3.82 Å) becomes weaker, demonstrating the existence of more disordered structure of **NOC6F-2** in the active layer. In the in-plane direction, the PBDB-T:**NOC6F-1** blend film presents a stronger (100) peak at q_{xy} = 0.30 Å^{-1} (*d* = 21.03 Å) than that of PBDB-T:**NOC6F-2** one (q_{xy} = 0.30 Å^{-1}, *d* = 21.14 Å), indicating that more well-organized arrangement exists in the

blend film of **NOC6F-1**. Hence, when blended with PBDB-T, **NOC6F-1** exhibits more orderly stacking both along the out-of-plane and in-plane directions than **NOC6F-2**. The presence of orderly stacking along the out-of-plane for **NOC6F-1** is more favorable for charge transport.

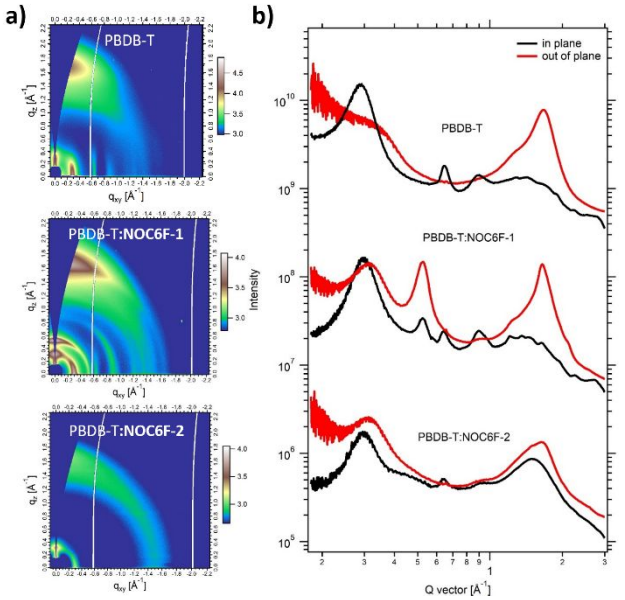

Fig. 4 a) 2D GIWAXS scattering patterns; and b) line profiles of PBDB-T pure film, PBDB-T:**NOC6F-1** and PBDB-T:**NOC6F-2** blend films.

Conclusion

In summary, we designed and synthesized two noncovalently fused-ring electron acceptors **NOC6F-1** and **NOC6F-2**, which are mutually isomers with the same side-chains and end-groups. The isomeric structures have a significant effect on the molecular stacking, absorption, charge transport and photovoltaic performances. Compared to **NOC6F-2**, **NOC6F-1** exhibits smaller distortions between cyclopentadithiophene units and the central naphthalene unit, which resulted in an extended conjugation and enhanced π-π stacking. The molecular backbone of **NOC6F-2** exhibits a poor planarity, which can restrict the delocalization of π electrons. When blending with PBDB-T, OSCs based on PBDB-T:**NOC6F-2** merely showed a PCE of 6.74% with low J_{sc} and FF. OSCs based on **NOC6F-1** achieved a higher J_{sc} of 17.08 mA cm^{-2} and an FF of 65.79%, thus leading to a significantly enhanced PCE of 10.62%. More importantly, our results have demonstrated that 2,6-linked naphthalene unit can be used as a core to synthesize NC-FREAs for high efficiency OSCs.

Experimental Section

The measurements and fabrication of the PSCs are described in the ESI.†

Conflicts of interest

The authors declare no conflicts of interest.

Acknowledgements

Financial support from the NSF of China (51933001, 21975031, 21574013, 21734009, 21421003, 21875182), the Beijing Natural Science Foundation (2182030), the Program for Changjiang Scholars and Innovative Research Team in University, and the Fundamental Research Funds for the Central Universities is gratefully acknowledged. 111 project 2.0 (BP2018008). X-ray data was acquired at beamlines 7.3.3 at the Advanced Light Source, which is supported by the Director, Office of Science, Office of Basic Energy Sciences, of the U.S. Department of Energy under Contract No. DE-AC02-05CH11231. The authors thank Chenhui Zhu at beamline 7.3.3 for assistance with data acquisition.

References

1 S. Feng, D. Ma, L. Wu, Y. Liu, C. Zhang, X. Xu, X. Chen, S. Yan, Z. Bo, *Sci. China Chem.*, 2018, **61**, 1320-1327.

2 X. Shi, X. Liao, K. Gao, L. Zuo, J. Chen, J. Zhao, F. Liu, Y. Chen and A. K. Y. Jen, *Adv. Funct. Mater.*, 2018, **28**, 1802324.

3 Z. Yao, X. Liao, K. Gao, F. Lin, X. Xu, X. Shi, L. Zuo, F. Liu, Y. Chen and A. K. Jen, *J. Am. Chem. Soc.*, 2018, **140**, 2054-2057.

4 H. H. Gao, Y. Sun, X. Wan, X. Ke, H. Feng, B. Kan, Y. Wang, Y. Zhang, C. Li and Y. Chen, *Adv. Sci.*, 2018, **5**, 1800307.

5 S. Dai, F. Zhao, Q. Zhang, T. K. Lau, T. Li, K. Liu, Q. Ling, C. Wang, X. Lu, W. You and X. Zhan, *J. Am. Chem. Soc.*, 2017, **139**, 1336-1343.

6 J. Jia, N. Zheng, Z. Wang, Y. Huang, C. Duan, F. Huang and Y. Cao, *Sci. China Chem.*, 2017, **60**, 1458-1467.

7 S. Li, L. Ye, W. Zhao, S. Zhang, S. Mukherjee, H. Ade and J. Hou, *Adv. Mater.*, 2016, **28**, 9423-9429.

8 Z. Luo, H. Bin, T. Liu, Z. G. Zhang, Y. Yang, C. Zhong, B. Qiu, G. Li, W. Gao, D. Xie, K. Wu, Y. Sun, F. Liu, Y. Li and C. Yang, *Adv. Mater.*, 2018, **30**, 1706124.

9 Y. Cui, H. Yao, J. Zhang, T. Zhang, Y. Wang, L. Hong, K. Xian, B. Xu, S. Zhang, J. Peng, Z. Wei, F. Gao and J. Hou, *Nat. Commun.*, 2019, **10**, 2515.

10 X. Xu, K. Feng, Z. Bi, W. Ma, G. Zhang and Q. Peng, *Adv. Mater.*, 2019, **31**, 1901872.

11 L. Hong, H. Yao, Z. Wu, Y. Cui, T. Zhang, Y. Xu, R. Yu, Q. Liao, B. Gao, K. Xian, H. Y. Woo, Z. Ge and J. Hou, *Adv. Mater.*, 2019, 1903441.

12 L. Meng, Y. Zhang, X. Wan, C. Li, X. Zhang, Y. Wang, X. Ke, Z. Xiao, L. Ding, R. Xia, H.-L. Yip, Y. Cao and Y. Chen, 2018, *Science*, **361**, 1094-1098.

13 F. Huang, Z. Bo, Y. Geng, X. Wang, L. Wang, Y. Ma, J. Hou, W. Hu, J. Pei, H. Dong, S. Wang, Z. Li, Z. Shuai, Y. Li and Y. Cao, *Acta Polym. Sin.*, 2019, **10**, 988–1046.

14 H. Yao, Y. Chen, Y. Qin, R. Yu, Y. Cui, B. Yang, S. Li, K. Zhang and J. Hou, *Adv. Mater.*, 2016, **28**, 8283-8287.

15 Y. Li, L. Zhong, B. Gautam, H.-J. Bin, J.-D. Lin, F.-P. Wu, Z. Zhang, Z.-Q. Jiang, Z.-G. Zhang, K. Gundogdu, Y. Li and L.-S. Liao, *Energy Environ. Sci.*, 2017, **10**, 1610-1620.

16 R. Hou, M. Li, J. Wang, Z. Bi, S. Feng, X. Xu, W. Ma and Z. Bo, *J. Mater. Chem. C*, 2019, **7**, 3335-3341.
17 Q. An, W. Gao, F. Zhang, J. Wang, M. Zhang, K. Wu, X. Ma, Z. Hu, C. Jiao and C. Yang, *J. Mater. Chem. A*, 2018, **6**, 2468-2475.
18 P. Jiang, H. Lu, Q.-Q. Jia, S. Feng, C. Li, H.-B. Li and Z. Bo, *J. Mater. Chem. A*, 2019, **7**, 5943-5948.
19 Y. Yang, Z. G. Zhang, H. Bin, S. Chen, L. Gao, L. Xue, C. Yang and Y. Li, *J. Am. Chem. Soc.*, 2016, **138**, 15011-15018.
20 J. Yuan, Y. Zhang, L. Zhou, G. Zhang, H.-L. Yip, T.-K. Lau, X. Lu, C. Zhu, H. Peng, P. A. Johnson, M. Leclerc, Y. Cao, J. Ulanski, Y. Li and Y. Zou, *Joule*, 2019, **3**, 1140-1151.
21 Y. Lin, J. Wang, Z. G. Zhang, H. Bai, Y. Li, D. Zhu and X. Zhan, *Adv. Mater.*, 2015, **27**, 1170-1174.
22 H. Bai, Y. Wang, P. Cheng, J. Wang, Y. Wu, J. Hou and X. Zhan, *J. Mater. Chem. A*, 2015, **3**, 1910-1914.
23 Z. Fei, F. D. Eisner, X. Jiao, M. Azzouzi, J. A. Rohr, Y. Han, M. Shahid, A. S. R. Chesman, C. D. Easton, C. R. McNeill, T. D. Anthopoulos, J. Nelson and M. Heeney, *Adv. Mater.*, 2018, **30**, 1705209.
24 W. Li, M. Chen, J. Cai, E. L. K. Spooner, H. Zhang, R. S. Gurney, D. Liu, Z. Xiao, D. G. Lidzey, L. Ding and T. Wang, *Joule*, 2019, **3**, 819-833.
25 S. Feng, C. Zhang, Z. Bi, Y. Liu, P. Jiang, S. Ming, X. Xu, W. Ma and Z. Bo, *ACS Appl. Mater. Interfaces*, 2019, **11**, 3098-3106.
26 Y. Li, X. Liu, F.-P. Wu, Y. Zhou, Z.-Q. Jiang, B. Song, Y. Xia, Z.-G. Zhang, F. Gao, O. Inganäs, Y. Li and L.-S. Liao, *J. Mater. Chem. A*, 2016, **4**, 5890-5897.
27 J. Zhu, Z. Ke, Q. Zhang, J. Wang, S. Dai, Y. Wu, Y. Xu, Y. Lin, W. Ma, W. You and X. Zhan, *Adv. Mater.*, 2018, **30**, 1704713.
28 X. Guo, J. Quinn, Z. Chen, H. Usta, Y. Zheng, Y. Xia, J. W. Hennek, R. P. Ortiz, T. J. Marks and A. Facchetti, *J. Am. Chem. Soc.*, 2013, **135**, 1986-1996.
29 H. Huang, L. Yang, A. Facchetti and T. J. Marks, *Chem. Rev.*, 2017, **117**, 10291-10318.
30 Y. Liu, Z. Zhang, S. Feng, M. Li, L. Wu, R. Hou, X. Xu, X. Chen and Z. Bo, *J. Am. Chem. Soc.*, 2017, **139**, 3356-3359.
31 S. Li, L. Zhan, F. Liu, J. Ren, M. Shi, C. Z. Li, T. P. Russell and H. Chen, *Adv. Mater.*, 2018, **30**, 1705208.
32 D. Liu, B. Kan, X. Ke, N. Zheng, Z. Xie, D. Lu and Y. Liu, *Adv. Energy Mater.*, 2018, **8**, 1801618.
33 Y. Liu, M. Li, X. Zhou, Q.-Q. Jia, S. Feng, P. Jiang, X. Xu, W. Ma, H.-B. Li and Z. Bo, *ACS Energy Lett.*, 2018, **3**, 1832-1839.
34 Y.-Q.-Q. Yi, H. Feng, N. Zheng, X. Ke, B. Kan, M. Chang, Z. Xie, X. Wan, C. Li and Y. Chen, *Chem. Mater.*, 2019, **31**, 904-911.
35 H. Huang, Q. Guo, S. Feng, C. Zhang, Z. Bi, W. Xue, J. Yang, J. Song, C. Li, X. Xu, Z. Tang, W. Ma and Z. Bo, *Nat. Commun.*, 2019, **10**, 3038.
36 I. Osaka, T. Abe, S. Shinamura and K. Takimiya, *J. Am. Chem. Soc.*, 2011, **133**, 6852-6860.
37 J. Wang, J. Zhang, Y. Xiao, T. Xiao, R. Zhu, C. Yan, Y. Fu, G. Lu, X. Lu, S. R. Marder and X. Zhan, *J. Am. Chem. Soc.*, 2018, **140**, 9140-9147.
38 W. Wu, G. Zhang, X. Xu, S. Wang, Y. Li and Q. Peng, *Adv. Funct. Mater.*, 2018, **28**, 1707493.
39 D. Zhao, Q. Wu, Z. Cai, T. Zheng, W. Chen, J. Lu and L. Yu, *Chem. Mater.*, 2016, **28**, 1139-1146.
40 J. Song, C. Li, L. Ye, C. Koh, Y. Cai, D. Wei, H. Y. Woo and Y. Sun, *J. Mater. Chem. A*, 2018, **6**, 18847-18852.
41 J. Liu, S. Chen, D. Qian, B. Gautam, G. Yang, J. Zhao, J. Bergqvist, F. Zhang, W. Ma, H. Ade, O. Inganäs, K. Gundogdu, F. Gao and H. Yan, *Nat. Energy*, 2016, **1**, 16089.
42 D. Qian, Z. Zheng, H. Yao, W. Tress, T. R. Hopper, S. Chen, S. Li, J. Liu, S. Chen, J. Zhang, X. K. Liu, B. Gao, L. Ouyang, Y. Jin, G. Pozina, I. A. Buyanova, W. M. Chen, O. Inganas, V. Coropceanu, J. L. Bredas, H. Yan, J. Hou, F. Zhang, A. A. Bakulin and F. Gao, *Nat. Mater.*, 2018, **17**, 703-709.
43 D. Yang, Y. Wang, T. Sano, F. Gao, H. Sasabe and J. Kido, *J. Mater. Chem. A*, 2018, **6**, 13918-13924.
44 K. Vandewal, K. Tvingstedt, A. Gadisa, O. Inganäs and J. V. Manca, *Phys. Rev. B*, 2010, 81, 125204.
45 M. A. Green, *Prog. Photo.: Res. Appl.*, 2012, **20**, 472-476.
46 T. Liu, L. Huo, S. Chandrabose, K. Chen, G. Han, F. Qi, X. Meng, D. Xie, W. Ma, Y. Yi, J. M. Hodgkiss, F. Liu, J. Wang, C. Yang and Y. Sun, *Adv. Mater.*, 2018, **30**, 1707353.
47 H. Xin, F. S. Kim and S. A. Jenekhe, *J. Am. Chem. Soc.*, 2008, **130**, 5424-5425.
48 J. J. van Franeker, G. H. Heintges, C. Schaefer, G. Portale, W. Li, M. M. Wienk, P. van der Schoot and R. A. Janssen, *J. Am. Chem. Soc.*, 2015, **137**, 11783-11794.

TOC